ENVIRONMENTAL RESEARCH COMMUNICATIONS
INCLUSIVE PUBLISHING TRUSTED SCIENCE
PURPOSE-LED PUBLISHING™

PAPER • OPEN ACCESS

Enhancing selenium removal using pre-treated natural clay: experimental investigation and predictive modeling

To cite this article: Gude Ramesh *et al* 2024 *Environ. Res. Commun.* **6** 115010

View the article online for updates and enhancements.

You may also like

- The surface downward longwave radiation of the CMIP6 HighResMIP in East Asia offline corrected by the three-dimensional sub-grid terrain longwave radiative effect scheme
Chunlei Gu, Anning Huang, Xin Li et al.
- Modeling spatiotemporal land use/land cover dynamics by coupling multilayer perceptron neural network and cellular automata markov chain algorithms in the Wabe river catchment, Omo Gibe River Basin, Ethiopia
Yonas Mathewos, Brook Abate, Mulugeta Dadi et al.
- A Delphi study on identifying environmental risk factors in the construction of China-Pakistan Economic Corridor (CPEC)
Iqtidar Hussain, Sun Zhonggen and Israr Hussain

This content was downloaded from IP address 166.104.66.193 on 06/12/2024 at 04:46

Environmental Research Communications

PAPER

Enhancing selenium removal using pre-treated natural clay: experimental investigation and predictive modeling

Gude Ramesh[1,7], **Biswajit Ruj**[2,7], **Bhaskar Bishayee**[2], **Rishya Prava Chatterjee**[2], **Ramesh Kumar**[3,7], **Moonis Ali Khan**[4], **Byong-Hun Jeon**[3], **Jayato Nayak**[5,7] and **Sankha Chakrabortty**[6]

[1] National Institute of Advanced Manufacturing Technology NIAMT, Hatia, Ranchi, Jharkhand - 834003, India
[2] Material Structure and Evaluation Group, CSIR-Central Mechanical Engineering Research Institute, Durgapur-713209, West Bengal, India
[3] Department of Earth Resources & Environmental Engineering, Hanyang University, 222-Wangsimni-ro, Seongdong-gu, Seoul 04763, Republic of Korea
[4] Department of Chemistry, College of Science, King Saud University, Riyadh 11451, Saudi Arabia
[5] Centre for Life Science, Mahindra University, Hyderabad, Telangana 500043, India
[6] School of Chemical Technology, Kalinga Institute of Industrial Technology, Bhubaneswar-751024, Odisha, India
[7] Authors have equal contributions

E-mail: bhjeon@hanyang.ac.kr **and** sankha.nit@gmail.com

Keywords: Clay material, optimization, natural available waste material, pre-treatment, selenium adsorption

OPEN ACCESS

RECEIVED
20 August 2024

REVISED
10 October 2024

ACCEPTED FOR PUBLICATION
22 October 2024

PUBLISHED
20 November 2024

Original content from this work may be used under the terms of the Creative Commons Attribution 4.0 licence.

Any further distribution of this work must maintain attribution to the author(s) and the title of the work, journal citation and DOI.

Abstract

A heat treatment methodology was adopted as a pretreatment strategy, altering the porous structure of the clay to minimize leaching for selenium adsorption in an aqueous system. Rigorous experiments were carried out in batch mode to determine optimal parameters across various variables, including contact time, adsorbent dosages, selenium concentrations, pH, temperature, and stirring speed during selenium removal using natural clay. Investigating several kinetic and isotherm models revealed the best fitting for the pseudo-second-order and the Langmuir isotherm. Endothermic and spontaneous characteristics of the adsorption process were shown during thermodynamic analysis. In this study, a predictive model for the efficiency of selenium separation was established using Response Surface Methodology (RSM). Additionally, an Artificial Neural Network (ANN), a data-driven model, was employed for comparative analysis. The predictive model exhibited a high degree of agreement with experimental data, demonstrated by a low relative error of <0.10, a high regression coefficient of >0.97), and a substantial Willmott-d index of >0.95. Moreover, the efficacy of pre-activated clay in selenium removal was assessed, revealing the superior performance of ANN models over RSM models in forecasting the efficiency of the adsorption process. This research significantly advances an effective and sustainable material for selenium removal, providing valuable insights into predictive modeling techniques applicable to similar contexts to boost scale-up confidence during industrial implementation in affected regions.

1. Introduction

The concentration of selenium in water plays a crucial role in determining whether it serves as a vital element or poses a risk of toxicity (Janz 2011, Pommier *et al* 2019). In the realm of water quality regulations, divergent standards exist for selenium concentration. The United States mandates a permissible limit of 50 $\mu g\,l^{-1}$ in drinking water, while the European Union enforces a more stringent maximum threshold of 10 $\mu g\,l^{-1}$ (He *et al* 2018). Meanwhile, the World Health Organization (WHO) suggests a daily intake of 40 to 400 μg of selenium, stipulating a maximum allowable concentration of 40 $\mu g\,l^{-1}$ in drinking water (World Health Organization 2011). The escalating concern over selenium contamination in groundwater and wastewater has spurred the development of diverse removal methodologies. These encompass membrane-based processes, reduction techniques, adsorption, electrocoagulation, coagulation-flocculation, phytoremediation, co-precipitation, electrochemical approaches, chemical precipitation, and biological remediation strategies (Zheng *et al* 2014, Kalaitzidou *et al* 2020, Mora *et al* 2020, Malhotra *et al* 2020,

© 2024 The Author(s). Published by IOP Publishing Ltd

Table 1. The physical condition of clay minerals as a function of temperature (Crowley *et al* 2007).

Name Clay	Reversible transformation		Irreversible transformation	
	Normal clay	Anhydrous Clay	Anhydrous Clay	Anhydrous Clay
Structure	Crystalline	Crystalline	Amorphous	Re-crystallization
Temperature	⩽120 °C	120 °C–550 °C	550 °C–900 °C	⩾900 °C

Hamid *et al* 2021, Kushwaha *et al* 2021, Monei *et al* 2021, Mao *et al* 2024, Zhang *et al* 2024, Zhao *et al* 2024). Adsorption has emerged as a preeminent approach owing to its practicality in remote locations, cost-effectiveness, potential for sorbent renewal, and limited generation of detrimental sludge (Zoroufchi Benis *et al* 2020b). Various adsorbents, such as activated carbon, magnetic nanocomposites, chitosan-clay composites, modified sand, iron and aluminum oxides, and ion-imprinted polymers, have been employed for selenium remediation Kuan *et al* (1998), (Su *et al* 2008, Bleiman and Mishael 2010, Dobrowolski and Otto 2013, Mafu *et al* 2016, Lu *et al* 2017). However, there is a lack of cost-effective methods utilizing natural materials for selenium mitigation in contaminated water.

Clay minerals and waste materials have recently gained attention as alternatives to expensive commercial adsorbents like resins and activated carbon for water and wastewater treatment (Zoroufchi Benisa *et al* 2022). Clay minerals appeal due to their natural abundance, non-hazardous nature, reactivity, and low cost (Bibi *et al* 2016). However, studies have shown that during the adsorption process, undesirable components can leach from the inherent structure of these materials into the water despite their widespread availability and low cost (Zoroufchi Benisa *et al* 2022, Ruj *et al* 2022). Clay is composed of hydrous aluminosilicate with repeating units of two sheets of octahedron Al and tetrahedron $(Si_2O_5)^{2-}$. The edges of the octahedron consist of an O atom and groups of OH^- ions linked with cations, such as Al^{3+}, Mg^{2+}, and Fe^{2+}, forming hexagonal structures, which can be used as adsorbent either naturally or after some modifications (Khan *et al* 2023). The transformation temperatures of clay minerals depend on factors such as the content of impurity oxides, degree of crystallinity, particle sizes, heating duration, and the heating rate at specific temperatures (Lamberov *et al* 2012, Chakraborty 2014). Prolonged heating can induce reactions between clay's silica and alumina components, reducing solubility and promoting the development of crystalline phases. Additionally, extended heating may lead to particle or phase fusion, resulting in a lower leaching rate (Al-Zahrani and Abdul-Majid 2009, Mark *et al* 2019). In this study, natural clay was modified by heating it to approximately 550 °C for 90 min to enhance its adsorption capacity and minimize leaching. Temperature and holding time are crucial in modifying natural clay's heat treatment. Table 1 depicts the four main regions in which clays transform in relation to temperature (Crowley *et al* 2007).

Artificial neural networks (ANN) and response surface methodology (RSM) have recently become effective methods for modeling and optimizing various processes (Bishayee *et al* 2021, Kumar *et al* 2024, Pranjal *et al* 2024). Both RSM and ANN models provide useful insights when dealing with sophisticated separation processes that necessitate uncertain, multiple-variable analysis and extensive experiments. Based on statistical and mathematical methods, RSM is particularly useful for optimizing process uncertainties and evaluating their interdependencies. On the other hand, ANN, a type of artificial intelligence, can learn from input-output data and provide predictions even without detailed knowledge of the removal mechanisms.

This research aimed to develop the RSM model to forecast the maximum achievable percentage of selenium separation from an aqueous solution by leveraging naturally available waste material while operating under optimized conditions. Furthermore, the ANN-based model was employed to assess the significance of operational parameters and their interdependencies, facilitating process optimization with minimal margin for error. The RSM approach adopted the central composite design (CCD) to systematically investigate the influence of diverse operational factors, including the quantity of adsorbent used, contact duration, temperature, pH level, and selenium concentration, on the efficacy of sorption. Subsequently, the ANN model was deployed to validate the optimized parameters. The studies employed pseudo-first and second-order kinetics and the intra-particle diffusion model to evaluate the adsorption rate. The empirical data strongly aligned with the Freundlich adsorption isotherm model, substantiating the study's findings. Notably, the research uncovered the potential for efficient reusability of the adsorbent, signifying its viability for large-scale deployment in industrial settings to remove selenium from water.

Moreover, research reports on applying ANN and RSM models using low-cost materials for selenium removal, followed by cost evaluation studies, are scarce. The lack of such optimization studies for selenium remediation from drinking water using low-cost adsorbent materials in the existing literature results in difficulties in the scale-up of the process for its commercial implementation in affected regions. The novelty of the present study primarily resides in developing a cost-effective adsorbent utilizing naturally available clay

material for selenium separation. Furthermore, it involved optimizing process conditions through the synergistic application of RSM and ANN methodologies, culminating in a comprehensive cost evaluation.

2. Materials and methods

2.1. Chemicals

Selenium solution of 2% (v/v) HNO_3, Nickel (II) nitrate hex hydrate used as a modifier (Ni $(NO_3)_2$. $6H_20$, M = 290.81 g mol^{-1}), 100 ml and 250 ml volumetric flasks, 100 ml conical flasks and 50 ml measuring flask (Borosil, ISO 4788 In 27 °C), Micropipette(10–100 μL, LABQUEST Borosil), Whatman 41 filter paper (20 μm), filter funnel, REMI Revolutionary Centrifuge machine, (Model No; R-4C, SUPPLY: 220 V, 50 Hz, 1ØAC, RPM: 4000), conical centrifuge tubes of 15 ml, weighing machine(max.=220 g, Min.= 0.1 mg), the crucible, Muffle Furnace (220/230 V, AC Supply), pH adjustments were made by using 0.05 M NH_4OH and 0.1 M HCl.

2.2. Material collection and pretreatment

Clay was collected from Diamond Harbour near the Ganga River basin, India (Latitude 22.1927° N and Longitude 88.1895° E). The collected material was dried naturally under the sunlight, followed by oven drying at 105 °C to remove any moisture and achieve the constant weight before being sieved through a 60 μm sieve (Laub *et al* 2019). As previously stated, clay was modified by heat treatment in a furnace at 550 °C for 90 min.

2.3. Determination of selenium concentration through GF-AAS

The supernatant, containing the dissolved selenium, underwent filtration employing Whatman 41 filter paper to remove particulate matter and obtain a clarified solution. The quantification of selenium concentration within this solution was executed via Graphite Furnace - Atomic Absorption Spectroscopy (GF-AAS) (Model No: AA0S162302, Hallow Cathode Lamp, Se 15 mA, P/N:942339030341, Wave length:196 nm, Detection Limit: 0.8 $\mu g\,l^{-1}$), Thermo Fisher Scientific, iCE 3000 SERIES, AA Spectrometer. The adsorption capacity (μg/g) is calculated using the mass balance equation below

$$q_e = \frac{(C_o - C_e) * V}{W} \tag{1}$$

where q_e represents the amount of selenium adsorbed on NMC adsorbent (adsorption capacity) in μg/g; C_o and C_e are the equilibrium selenium concentrations before and after the adsorption experiment in μg/L; V and W are feed volume (in liter) and weight of adsorbent (in gram).

2.4. Analytical procedure for adsorbent characterizations

Characterizing the untreated and treated clay adsorbents involved various analytical techniques. Scanning electron microscopy coupled with energy-dispersive x-ray analysis (SEM-EDX) (JEOL Ltd, Japan) examined the adsorbent samples' morphology and elemental composition. Fourier Transform Infrared Spectroscopy (FTIR) was utilized to investigate the various functional groups (in adsorbent) through their discrete vibrational energy. Employing an IR Affinity-1S FT-IR Spectrophotometer (Shimadzu Co., Tokyo, Japan), a broad spectral range (400 to 4000 cm^{-1}) was analyzed to attribute characteristic spectra to various functional groups. Further characterization involved x-ray diffraction (XRD) using the Xpert Pro instrument from PAN Analytical in the UK. This method enabled the investigation of mineral phases present in the material, providing insights into its crystalline structure. N_2-based adsorption–desorption isotherms were also examined to evaluate the surface area and pore size distributions using Brunauer–Emmett–Teller (BET) and Barrett–Joyner–Halenda (BJH) analyzers (Quantachrome Nova 2200E, Florida). This analysis aided in understanding the material's surface characteristics and porosity. The utilization of this array of advanced characterization techniques facilitated a comprehensive understanding of the untreated and treated clay adsorbents, enabling insights into their structural, elemental, and surface properties crucial for their application in diverse industrial processes.

2.5. Batch experimental procedure

The experimental procedures involved conducting batch tests employing naturally heat-treated clay as an adsorbent to evaluate the influence of various operational factors, such as contact duration, adsorbent dosage, selenium concentration, solution pH, temperature, and agitation speed on selenium removal. By systematically varying each operational parameter while keeping others constant, the experiment aimed to identify the optimal conditions for selenium removal using heat-treated clay. This approach helps in identify key factors that enhance adsorption capacity and efficacy, thereby contributing valuable insights to the development of efficient water treatment solutions. This was accomplished by subjecting the solution to an oscillating motion in a temperature-controlled orbital shaker, consistently operating at a speed of 120 rpm until reaching adsorption

Table 2. Parameters and their level used for making CCD using RSM.

Factor	Parameters	Units	Min.	Max.	Coded Low	Coded High	Mean	Std. Dev.
A	Adsorbent dose	g/L	6	14	$-1 \leftrightarrow 8$	$+1 \leftrightarrow 12$	10	1.84
B	Contact time	Minutes	10	50	$-1 \leftrightarrow 20$	$+1 \leftrightarrow 40$	30	9.18
C	Selenium concentration	μg/L	50	450	$-1 \leftrightarrow 150$	$+1 \leftrightarrow 350$	250	91.77

Table 3. Weight percentage of the compositions present in natural clay and heat-treated clay.

S. No.	Elemental composition	% Weight			
		Natural Clay		Heat treated clay	
		Area 1	Area 2	Area 1	Area 2
1	C K	30.26	15.78	0	
2	O K	47.06	48.28	50.05	50.92
3	MgK	1.27	1.4	1.13	1.26
4	AlK	5.6	6.91	10.77	11.94
5	SiK	11.21	21.15	28.32	27.93
6	K K	1.3	1.79	2.42	3
7	CaK	0.32		0.88	
8	FeK	2.98	4.7	6.43	4.95

equilibrium. Post-treatment, the solution was left undisturbed overnight. The temperature remained constant at 27 °C throughout the entire experimental duration. The efficiency of selenium removal was calculated using the subsequent formula (Malhotra *et al* 2023):

$$\eta(\%) = \frac{C_o - C_e}{C_o} * 100 \tag{2}$$

Where C_o = initial selenium concentration in μg/L; C_e = equilibrium selenium concentration in μg/L.

2.6. Optimization studies

2.6.1. Response surface methodology-based optimization

RSM represents a suite of mathematical tools pivotal in delineating relationships between diverse independent factors and one or more responses in experimental settings (Chakraborty and Halder 2020). The statistical model generated by Design Expert Software (Version 6.0, Minneapolis, Stat-Ease, USA) was employed in all adsorption experiments. Three crucial parameters, namely contact time, initial selenium concentration, and adsorbent dose, acted as input variables, while the efficiency of selenium separation (%) using activated clay as the adsorbent served as the response variable. Other parameters, such as shaker speed (200 rpm), temperature (25 °C), and pH (7) were kept at constant values. The input variables' minimum (−1) and maximum (+1) values were 50 to 450 μg l^{-1} for selenium concentration, 6 to 14 g l^{-1} for adsorbent dose, and 10 to 50 min for contact time. Table 2 presents the coded table corresponding to these values. Table 3 illustrates the statistical experimental design formulated through Design Expert Software, predicated on multiple input factors. This design underwent evaluation employing the CCD technique, which was deemed the most appropriate RSM technique for experimental design scenarios. The model's efficacy was gauged based on R^2, Adjusted R^2, and Predicted R^2 values. A higher correlation coefficient (R^2) implies a more robust interpretation of the experimental dataset, validating the model's effectiveness.

2.6.2. Artificial neural network-based optimization

In ANNs, the fundamental components are nodes, which serve as interconnected computational units, each assigned a numerical value called a 'scalar weight' (w). The neuron's synaptic weight plays a crucial role in aggregating information from multiple sources and determines the potency of each incoming signal. Subsequently, these inputs are aggregated using an externally imposed scalar termed bias (Biswas *et al* 2018).

$$\text{Sum} = \sum_{i=0}^{n} x_i w_i \tag{3}$$

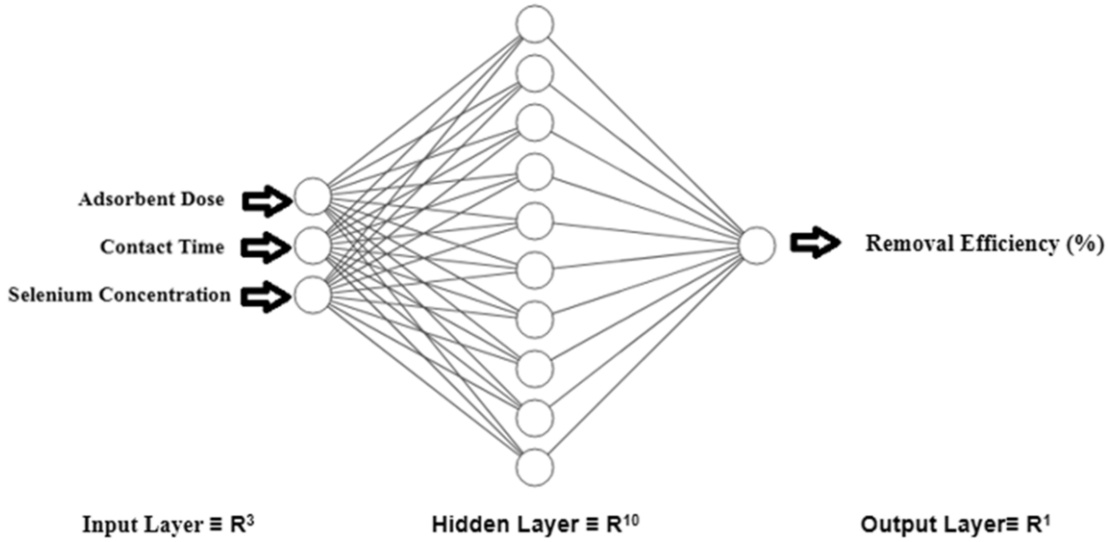

Figure 1. The Node diagram of ANN analysis 3-10-1.

The generation of the desired scalar output (denoted as 'o') within an ANN involves a crucial process: the transformation of the cumulative network output through an appropriate transfer function (represented as 'F'). In the particular scope of the referenced study, key factors serving as independent variables encompass selenium concentration, adsorbent quantity, and contact duration, significantly influencing the system's operational efficiency. The primary focus is assessing selenium removal efficacy, quantified as a percentage and graphically depicted in figure 1. Employing a layered feed-forward neural network (FNN) model, as detailed by Zendehdel *et al* (2017), constitutes the methodology. This FNN structure comprises distinct layers: an input layer receiving the variables, hidden layers for processing, and an output layer generating the anticipated results. Data can be transferred via the hidden layer from the input to the output layer. However, the current configuration of the ANN prohibits the introduction of additional lateral and feedback connections. The Leverberg-Marquardt technique was employed to iteratively adjust the internal network parameters, denoted as 'b' and 'w' to reduce the Mean Squared Error (MSE) function. The MSE can be calculated as follows.

$$\mathrm{MSE} = \sum_{i=0}^{n} \mathrm{Y_{i,observed}} - \mathrm{Y_{i,predicted}} \tag{4}$$

where $Y_{i,\ predicted}$ and $Y_{i,\ observed}$ are the experimental outputs (predicted and target, respectively); n defines the number of runs. The information from the experiments that made up the ANN Model is displayed in table 2. The data from the experiments were randomly split into three sets: training, testing, and validation. In the training phase, when the neural network is excessively trained, it exhibits reduced errors in the training data. As the training of the intricate neural network advances, it begins to assimilate superfluous noise signals alongside the initial input signals. This phenomenon degrades the network's generalization capabilities, impeding its accuracy in predicting outcomes on novel or uncharted data instances. An 'Early Stopping Approach' is deployed to counteract the detrimental effects of overfitting, promptly discontinuing the training procedure at the onset of indications wherein the validation error escalates. Subsequently, the network's reliability is gauged through rigorous testing, while the efficacy of the ANN model is appraised by scrutinizing its performance against validation metrics.

2.7. Error analysis

A comprehensive comparison of the performance of the RSM and ANN models was conducted through rigorous statistical analysis, employing three key metrics: the Coefficient of Determination (R^2), Relative Error (RE), and the Willmott d-index (d_{index}). The statistical evaluation was carried out by utilizing both the model-generated data and the empirically observed data, employing a widely accepted standard statistical approach, namely, the relative error analysis. This analysis procedure involves the assessment of specific parameters, as outlined in the subsequent criteria:

The following expression was used to calculate RMSE (Root mean square error):

$$\mathrm{RMSE} = \left(\sum_{N=1}^{n} (P_N - E_N)^2 / N \right)^{1/2} \tag{5}$$

Where P_N and E_N are the numbers of model findings and experimental findings generated from the RSM or ANN model.

Then, relative error (RE) was calculated

$$\mathrm{RE} = (\mathrm{RMSE}/E_{mean}) \tag{6}$$

E_{mean} represents the average value of experimental data.

i. To enhance the model efficiency, the Willmott d-index (d_{will}) approach was used, which was evaluated as follows:

$$d_{index} = 1 - \left\{ \left(\sum_{N=1}^{n} (P_N - E_N)^2 \right) \right\} \Big/ \left(\sum_{N-1}^{n} [|(P_N - E_{mean})| + |(P_N - E_{mean})|]^2 \right) \tag{7}$$

ii. The following expression was used to determine the value of the regression coefficient (R^2):

$$R^2 = \frac{A_{xy}^2}{P_x^2 * P_y^2} \tag{8}$$

Where A_{xy}^2 represents the covariance among independent and dependent variables, P_x^2 represents the variance of the variables dependent on the independent variables, and P_y^2 represents the variance of the independent variables.

2.8. Adsorption isotherms

Adsorption isotherms depict the equilibrium state of solute molecules in the liquid and bonded (with adsorbent) phases (Mourabet *et al* 2011). The batch experiments were conducted to optimize the initial selenium concentration for a 30-minute equilibrium time at a pH of 7 and a temperature of 27 °C. Each conical flask of 50 ml selenium solution with varied concentrations ranging from 50 to 400 $\mu g\,l^{-1}$ was agitated at 120 rpm with a predetermined adsorbent dose. Then, the solution was filtered to ascertain the selenium concentration. The optimum concentration was found to be 250 $\mu g\,l^{-1}$. The acquired data were fitted into two regularly used isotherms, Langmuir (1918) and Freundlich (1907), to better understand adsorption isotherms. The linear equations of Langmuir and Freundlich are as follows,

$$\frac{1}{q_e} = \frac{1}{K_L \cdot q_{max}} \frac{1}{C_e} + \frac{1}{q_{max}} \tag{9}$$

$$\log q_e = \log K_f + \frac{1}{n} \log C_e \tag{10}$$

The equation presented describes the adsorption process involving selenium onto a solid surface. In this context, 'q_e' represents the quantity of selenium sorbed per unit mass of the sorbent material (μg/g), while 'C_e' denotes the equilibrium concentration of selenium in the raffinate (μg/L). Langmuir's 'q_{max}' and 'K_L' constants show adsorption capacity (μg/g) and maximum monolayer sorption efficiency (L/μg). Additionally, 'K_f' stands for the Freundlich constant (μg/g), and 'n' signifies the constant related to the adsorption intensity. The Langmuir isotherm, characterized by these constants, encapsulates essential properties governing adsorption. The dimensionless equilibrium parameter (R_L), introduced by Weber and Chakravorti (1974), is fundamental in understanding the Langmuir model. This parameter is defined as:

$$R_L = \frac{1}{1 + K_L \cdot C_i} \tag{11}$$

where K_L and C_i indicate the Langmuir constant (L μ/g) and initial selenium concentration (μg/L).

2.9. Adsorption kinetics

A kinetic investigation was carried out to determine the time required for achieving optimal selenium adsorption onto thermally treated clay, serving as an adsorbent, under specific conditions of pH 7 and a temperature of 27 °C. The experiment employed a known dosage of 10 $g\,l^{-1}$ of the adsorbent in conical flasks, each containing 50 ml of selenium solution with a fixed feed concentration of 50 $\mu g\,l^{-1}$ and stirred at 120 rpm.

Samplings were done at fixed intervals within a 210-minute duration, and the selenium concentration was measured to track the adsorption process. The initial stages of the process exhibited rapid removal of selenium, reaching equilibrium within 30 min. The kinetic data were analyzed using various models, such as pseudo-first and second-order (Lagergren 1898, Ho and McKay 1999) and intra-particle diffusion, and the resultant data were expressed as linear equations to characterize the process. These models were utilized to elucidate the kinetics of selenium adsorption onto heated clay as an adsorbent under pH 7 and a temperature of 27 °C. The resulting linear equations describing the adsorption process are given below.

$$\ln(q_e - q_t) = \ln q_e - K_1 t \tag{12}$$

$$\frac{t}{q(t)} = \frac{1}{K_2 q_e^2} + \frac{t}{q_e} \tag{13}$$

$$q_t = K_i t^{0.5} + C \tag{14}$$

Here, 'q_e' represents the adsorption capacity (μg/L) at equilibrium; 'q_t' indicates the adsorption capacity at any given time 't', 'K_1' and 'K_2' denote the rate constants for the Pseudo first and second-order reactions, respectively, and 'K_i' signifies the rate constant for intra-particle diffusion in units of μg/g $h^{0.5}$.

2.10. Thermodynamic study

Adsorption tests were performed at 298 K, 303 K, and 318 K to assess thermodynamic variables like change in Gibbs free energy (ΔG°), which indicates whether the adsorption process is spontaneous or not, and changes in entropy (ΔS°) and enthalpy (ΔH°) to confirm the exothermic or endothermic process.

Change in Gibbs free energy (Wasewar *et al* 2009) determined by using the equation as follows,

$$\Delta G^0 = RT\ln(K_L) \tag{15}$$

R and K_L, show the ideal gas (8.314 J mol^{-1} K^{-1}), the equilibrium adsorption constants, and T stands for the temperature (K).

The changes in enthalpy (ΔH°) and entropy (ΔS°) were estimated by (Badawy *et al* 2010) following Van't Hoff equation as follows

$$\ln K_L = \frac{\Delta S^0}{R} - \frac{\Delta H^0}{RT} \tag{16}$$

Where ΔH° (kJ/mol) is measured by the intercept and ΔS° (kJ/mol) is determined by the slope of 1/T Vs $\ln K_L$ plot

3. Results and discussion

3.1. Characterizations of the adsorbents

SEM images investigated the physical characteristics and alterations of the adsorbent surface before and after the heat treatment of clay. Figure 2 shows the SEM images of natural clay (figure 2(a)) and clay that underwent a heat treatment (figure 2(b)). What becomes immediately apparent is a porous, rugged, distorted, and frayed structure on the surface of the natural clay. This visual representation underscores the intricate and irregular nature of the natural clay's surface. Conversely, the SEM image of the heat-treated clay paints a different picture altogether, revealing smooth surfaces adorned with porous nanoparticles. The heat treatment process appears to have transformed the clay's surface into a more uniform and refined state than its natural counterpart. However, it is crucial to note that an unintended consequence of this transformation occurred, resulting in the aggregation or clumping together of the nano-sorbent particles. This phenomenon can be attributed to the Van der Waals forces, which are attractive forces that operate between molecules or particles when they are nearby. In this case, these forces caused the nano-sorbent particles to come together, forming agglomerations.

EDX analysis was conducted on both natural and heated clay to ascertain the changes in the chemical composition of the clay substance. Distinct areas were selected for analysis in both types of clay, as presented in table 3, which confirmed the major constituents of C, O, Al, and SiO_2. Minor quantities of Mg, Ca, Fe, and K are also observed. By examining the EDX, it was observed that there was a significant increase in carbon and silica concentrations in area 2 compared to area 1 in natural clay. In the case of heat-treated clay, the main components were SiO_2, O, and Al, with smaller amounts of Mg, K, Fe, and Ca. Analysis of the EDX data revealed a significant increase in oxygen concentration in area 2 of the heated clay compared to area 1 (table 3). Moreover, smaller increases were observed for Al, SiO_2, and K. Interestingly, the carbon percentage disappeared after heating in natural and heated clay. However, after the clay was activated, there was an improvement in the amount of Al, SiO_2, and Fe, increasing from 5.6%, 11.21%, and 2.98% to 11.94%, 27.93%, and 4.95%,

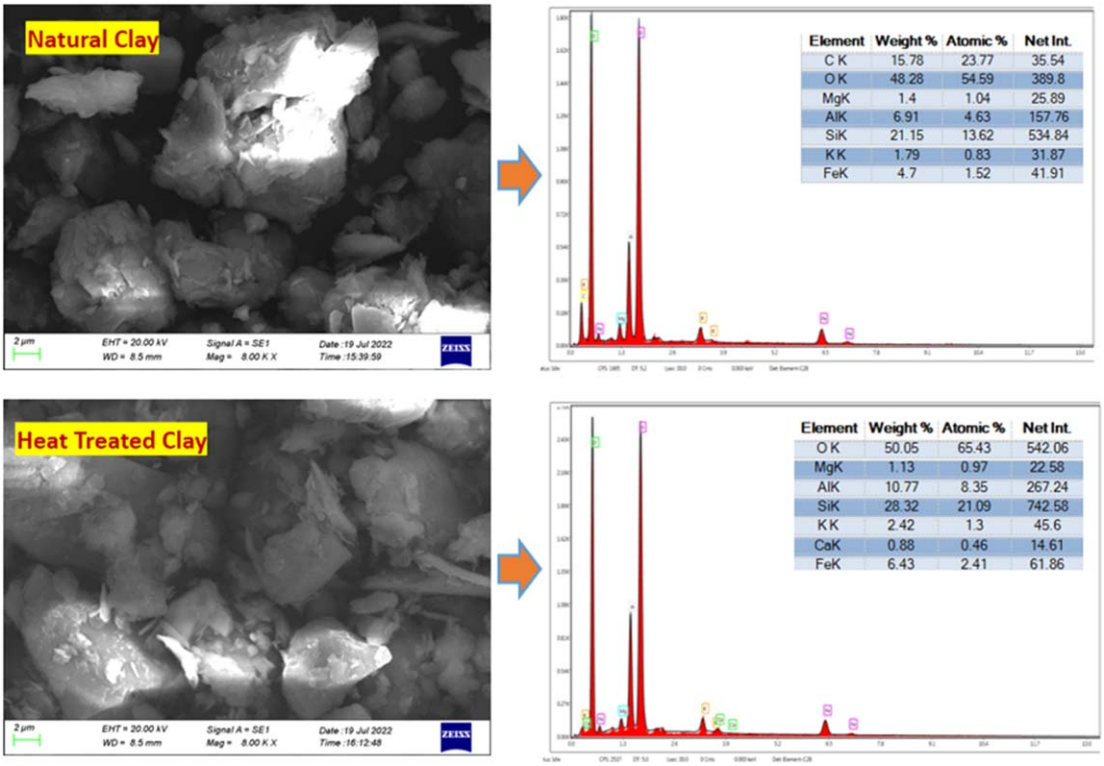

Figure 2. SEM-EDX-based morphological analysis of natural clay (a) and heat-treated clay (b).

respectively. It is possible that the sintering of the clay material contributed to the disappearance of carbon in the activated clay.

Understanding the adsorption process requires a proper understanding of the chemical structure of the adsorbent material, as it strongly influences the adsorption capacity and surface characteristics of the adsorbents. Carbon–oxygen groups are particularly significant structures that impact the surface behavior of adsorbents. The FTIR characterization technique is valuable for identifying characteristic functional groups essential for Se (IV) adsorption. The 400 to 4000 cm^{-1} spectral region, the FTIR spectra of natural and heated clay were captured (figures 3(a) and (b)). Previous studies on kaolinite clay have revealed similar characteristic bands appearing at 3,618.67, 3,641.59, 1,100.39, 907.602, 830.38, 758.355, 521.24, and 456.84 cm^{-1} (Hajjaji *et al* 2001). The presence of both free and hydrogen bound OH groups on the adsorbent surface is shown by a broad band between 3100 and 3700 cm^{-1} in all adsorbents (Wasewar *et al* 2009).

The significance of this range lies in its capacity to offer profound insights into the composition and surface characteristics of the adsorbents under scrutiny. Across all the evaluated adsorbents, a consistently observable broadband within this spectral region stands out. This distinct band serves as a clear indicator of the existence of specific chemical groups recognized as hydroxyl (OH) groups residing on the surfaces of these materials. These OH groups manifest in two discernible forms: 'free' OH groups and OH groups bound by hydrogen. Their presence carries particular intrigue due to their pivotal role in these materials' surface adsorption processes. Understanding the presence and behavior of these OH groups is vital as they significantly influence the adsorption mechanisms at the material's surface. The broad stretching observed in this spectral range is associated with the vibrations of these OH groups. Notably, these OH^- groups are involved in hydrogen bonding interactions with oxygen atoms bound to silicon (O–Si) on the adsorbent's surface.

Furthermore, another peak was observed at 3624.9 cm^{-1}, corresponding to the surface's adsorbed water molecules. This peak's presence suggests that water molecules also interact with the adsorbent material, likely through hydrogen bonding. What's particularly intriguing is that even after sintering, which involves heating the natural clay material to high temperatures, the resulting spectrum still displays the characteristic peaks associated with O-H stretching and bending vibrations. This persistence of O-H-related peaks suggests that the sintered natural clay maintains its hydroxyl groups and hydrogen bonding interactions even after undergoing this thermal treatment. This indicates that the natural clay utilized for the investigation can be categorized as phyllosilicate because the structural unit layer contains inner hydroxyl groups. The disappearance of the 3697.5 cm^{-1} band may be attributed to sintering at 550 °C (den Hartog *et al* 2014). At 1,036.39 and 456.20 cm^{-1}, characteristic bands of montmorillonite-Na were found (Madejova 2003). The high-intensity peak value

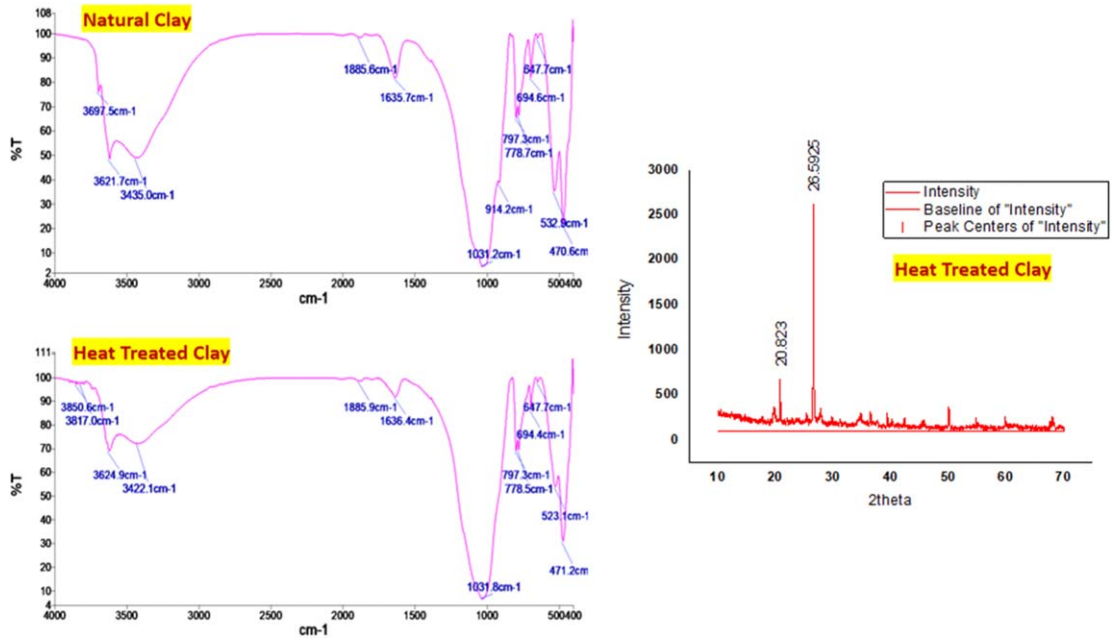

Figure 3. FTIR analysis of natural clay (a) and heat-treated clay (b), and XRD analysis of the heat-treated clay (c).

confirms the presence of this mineral concentration in the sample at 1031.2 cm^{-1}. Si-O stretching is associated with the band at 1,036.39 cm^{-1}, while Si–O–Si bending vibrations are associated with the band at 456.20 cm^{-1} (Gadsden 1975). Significantly, following the sintering process, it was observed that the mineral structures remained unaltered, specifically evident through the persistence of the 1031.8 cm^{-1} band in the spectra. This particular band is associated with various vibrations, including Si-O-Al, Si-O-Mg, Si–O–Si, and bending vibrations, denoted by the bands at 797.3 cm^{-1}, 523.1 cm^{-1}, and 471.2 cm^{-1}, respectively. These functional groups point to a substantial portion of the layer charge originating from substituting trivalent ions (Al^{3+} and Fe^{3+}) with divalent ions (Mg^{2+}) within the octahedral sheet. Such functional groups are commonly encountered in silicate minerals such as kaolinite and montmorillonite (Djebbar *et al* 2012). The stretching vibrations attributed to water molecules adsorbed on the heated clay surface are represented by the band at 3,422.41 cm^{-1} in the FTIR spectra. Additionally, a characteristic band, typically manifesting within the 1,650^{-1},600 cm^{-1} range and associated with the bending vibrations of adsorbed water, is observed at 1635.7 cm^{-1} as a medium-intensity band. Furthermore, the vibrations originating from surface hydroxyl groups (Si-Si-OH or Al-Al-OH) are discernible at 3624.9 cm^{-1} and 3422.1 cm^{-1}. Lastly, the presence of the 914.2 cm^{-1} band can be attributed to Al-O-OH and may be linked to the deformation of inner hydroxyl groups.

Figure 3(c) displays the XRD pattern of the heat-treated clay material. The XRD analysis revealed distinct peaks in the pattern. Formation of β-quartz in the clay after heat treatment is shown by the x-ray diffraction (XRD) pattern, which shows through the strong peaks at 20.823° and 26.59° (Sun *et al* 2016). These peaks are indicative of the β-quartz phase and relate to particular crystallographic planes (Nigay *et al* 2017). β-quartz, a polymorph of quartz that occurs at high temperatures, is created when clay is heated to a certain point. Significant changes in the crystalline structure of the clay have been generated by the heat treatment method, as indicated by the transformation to β-quartz. Results indicates that clay minerals can undergo high-temperature thermal treatment and form novel crystalline phases. Their effects on the material's properties and possible uses make an understanding of these structural changes critical. One way that heat treatment might improve the mechanical characteristics of clay-based ceramics is by causing amorphous phases to densify and crystallize.

The pore diameter distribution and specific surface area of activated natural clay were investigated using nitrogen adsorption–desorption isotherms. This analysis provides valuable information about the properties and structure of the clay material. Figure 3 shows the BET analysis findings, including a linear plot and the N_2 adsorption–desorption isotherm. The isotherm depicted in figure 4(a) corresponds to a type IV isotherm, indicating the presence of a micropore structure within the clay material. The size of these micropores ranges from 1.5 to 100 nanometers. By examining the graph, it can be observed that the relative pressure (P/P_o) range of 0.2–0.9 exhibits a consistent increase in nitrogen adsorption. The pore radius is 1.6 nanometers, further supporting a micropore structure in the activated clay material (Tang *et al* 2019). Figure 4(b) represents a linear BET plot, which provides information about the slope, intercept, and correlation values. The positive intercept value indicates that the material is microporous. Through the BET analysis, several critical parameters of the

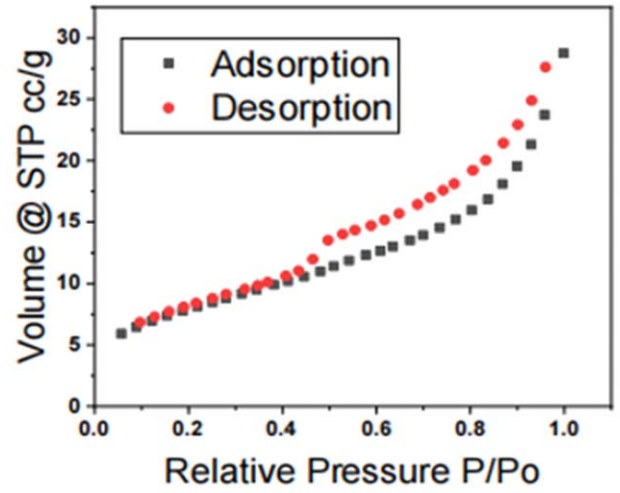

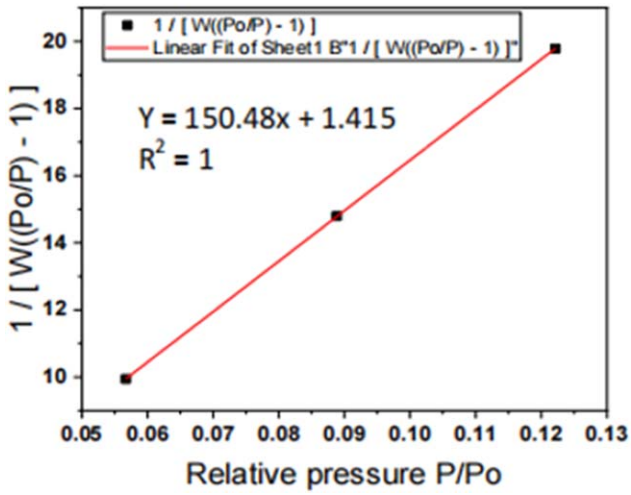

Slope	150.481 1/g
Intercept	1.415e+00 1/g
Correlation coefficient, R^2	1
C constant	107.317
Surface area	22.927 m^2/g
Pore radius	16.012 A°
Pore volume	0.035 cc/g

Figure 4. Surface area analysis of N_2 adsorption–desorption isotherm (a) BET plot (b).

adsorbent are determined. The surface area is calculated to be 22.927 $m^2\,g^{-1}$, the pore volume is 0.035 $cm^3\,g^{-1}$, and the pore radius is 16.012 Å. These results contribute to a comprehensive understanding of the activated clay material's characteristics and potential applications.

3.2. Effects of various operating parameters on selenium adsorption efficiency

The effect of different amounts of adsorbent, ranging from 2.5 to 30 g l^{-1}, on selenium uptake onto heated clay was investigated through a series of batch studies while maintaining a constant feed concentration (figure 5(a)). The highest adsorption efficiency (92%) was observed at an adsorbent dosage of 15 g l^{-1}, with a slightly lower efficiency of 90.6% at 10 g l^{-1}. The feed concentration used for this study was 250 μg l^{-1}, and applying 10 g l^{-1} of adsorbent resulted in a residual concentration of about 27 μg l^{-1}, falling below the WHO-recommended maximum concentration range (40 μg l^{-1}) for selenium. Thus, 10 g l^{-1} of adsorbent was selected for further investigation. A similar kind of study was showed that an adsorbent dose of 25 mg was the most effective way to remove 95.6% of selenium under the following conditions: a pH of 8.5, a contact time of 60 min, and an initial selenium concentration of 1 mg l^{-1} (Qureshi *et al* 2022). Initially, the removal of Selenium by the adsorbent increased as the adsorbent dosage increased, reaching an optimal dosage where the removal became constant. This trend was also observed when granular activated carbon (GAC) was used for Se (IV) removal, suggesting that the higher adsorbent dosages provided more adsorption sites and increased surface area (Wasewar *et al* 2009). In subsequent batch studies with a fixed adsorbent dosage of 10 g l^{-1}, the impact of different contact times (ranging from 15 to 210 min) on the uptake of Selenium onto heated clay was examined (figure 5(b)). The results revealed that the initial removal of selenium species from the aqueous solution using the adsorbent was very rapid. Similar fast rates were observed for Se (IV) removal using GAC and PAC, achieving over 61% and 43% removal within the first 10 min (Wasewar *et al* 2009). This was attributed to the abundance of unoccupied surface sites accessible during the early phases of the adsorption. However, as time progressed, the remaining

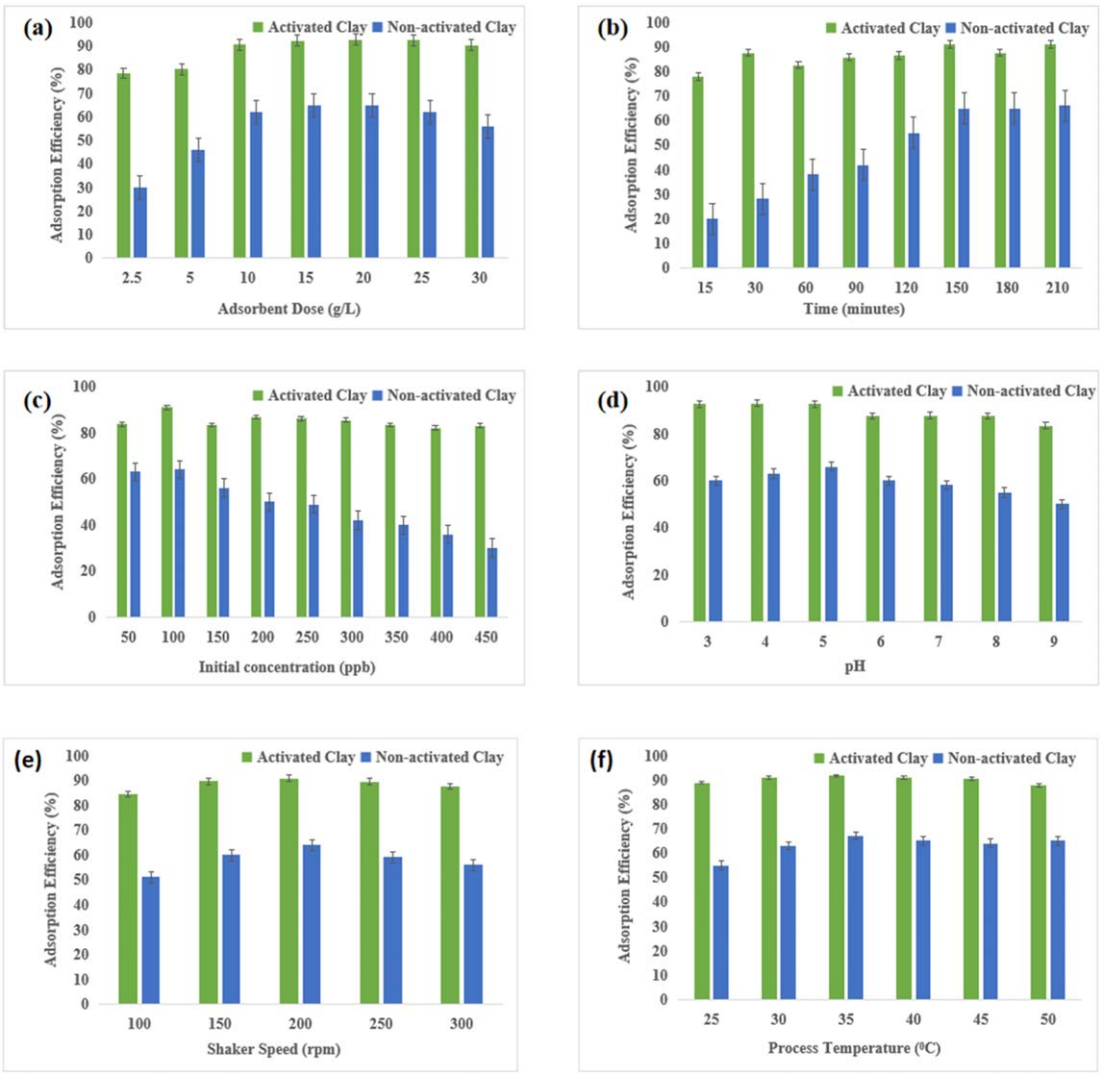

Figure 5. Effect of (a) adsorbent dosage (b) contact time (c) initial concentration (d) feed solution pH (e) Shaker speed (f) Temperature on selenium removal efficiency.

vacant surface sites became more challenging due to repulsive forces between solute molecules in the solid and liquid phases (Wasewar *et al* 2009). The adsorption rate of selenium species using adsorbent (heated clay) was exceptionally rapid, achieving an efficiency of over 88% within less than 30 min. As a result, all subsequent batch experiments in aqueous solutions were conducted with an optimal contact time of 30 min.

Researchers conducted batch studies using a fixed dose and time to assess the influence of different initial concentrations on selenium uptake onto heated clay. The investigated initial concentrations ranged from 50 to 450 $\mu g\,l^{-1}$. The results (which) depict the relationship between initial concentrations and Selenium uptake, are presented in figure 5(c). As the initial concentration of selenium increased, there was a slight decrease in efficiency. This finding aligns with a study conducted by Bleiman and Mishael (2010), where they investigated the removal of selenate from groundwater using chitosan clay composites (Al-oxides and Fe-oxides). In another study, the efficiency of selenium removal reduced as the original concentration also rose. It was shown that the elimination effectiveness was 95.6% when the initial concentration was 1 ppm, but it reduced to 85% when the concentration was increased to 5 ppm (Lichtfouse *et al* 2022). The decrease in efficiency can be attributed to the limited availability of adsorption sites at higher concentrations, which hinders effective adsorption. As a result, a significant proportion of selenium species remains in solution without binding to the adsorbent. However, even at an initial concentration of 250 $\mu g\,l^{-1}$, the remaining concentration remained within the maximum level recommended by the WHO, and the process achieved an optimal efficiency of 91%. Furthermore, additional batch studies were conducted with a fixed dose, time, and initial concentration to explore the impact of different pH values on selenium uptake onto heated clay. Figure 5(d) illustrates the variations in pH values from 3 to 9, reflecting the findings of adsorption capacity. The pH of a solution can considerably influence the adsorption efficacy of selenium. As the pH rose, the removal rate of selenium species

diminished, achieving optimal efficiency at a pH of 3. A study found that a low pH enhanced selenite adsorption, with optimal removal occurring at a pH of 6 (Arslan *et al* 2023). Parida *et al* (1997) found that the distinctive anionic behavior of SeO_3^{2-} species accounted for similar trends in cases of SeO_3^{2-} adsorption onto iron oxyhydroxides and ferrihydrite. According to Rovira *et al* (2008), the sorption edge for SeO_3^{2-} was shown to correspond with the predominance of $HSeO^{3-}$ in goethite and hematite adsorption tests. This finding is consistent with the current findings. The pH of the solution significantly affects the existence of Se anions due to the diprotic nature of selenic (H_2SO_4) and selenious (H_2SeO_3) acids. Typically, the pH of natural waters ranges from 5.0 to 9.0. The most prevalent forms are Se (IV) species like biselenite ($HSeO^{3-}$), selenite (SeO_3^{2-}), and Se (VI) species like SeO_4^{2-} (Torres *et al* 2010). The biselenite ion prevails in water within the pH range of 3.5 to 9.0, while SeO_3^{2-} dominates above pH 9.0. Selenious acid (H_2SeO^3) prevails at pH values below 3.5 (Wasewar *et al* 2009), and SeO_4^{2-} species are predominant under highly oxidizing conditions (Torres *et al* 2010). Similar to the adsorption of selenium using GAC, At alkaline pH, selenite adsorption reduces due to a decline in the fraction of an aqueous $HSeO^{3-}$ species (Wasewar *et al* 2009). Considering the significance of drinking water, a pH range of 6.5–8.5 is recommended, and an optimal removal efficiency of over 88% was achieved at a pH of 7. The effect of various shaker speeds ranging from 100 to 300 rpm on Selenium uptake onto heated clay was investigated in batch studies with a known dose, time, feed concentration, and pH. The results obtained with different shaker speeds are illustrated in figure 5(e). It was observed that the adsorption of Selenium increased with the increasing shaker speed up to a certain point, beyond which it started to decrease. The optimal efficiency was achieved at a shaker speed of 200 rpm. Furthermore, the effect of various temperatures ranging from 25 °C to 50 °C on selenium uptake onto heated clay was explored in batch studies with a known dose, time, feed concentration, shaker speed, and pH. Figure 5(f) shows the findings obtained at various temperatures. It was found that between 25 °C to 50 °C, there was no significant effect on the removal efficiency of selenium. A major influence on the adsorption effectiveness of selenium can be attributed to temperature, according to the previous report. As an illustration, a study discovered that elevating the temperature from 25 °C to 35 °C resulted in a 15% increase in the adsorption potential of selenium. Nevertheless, the temperature was not much improved by increasing it further than 35 °C.

3.3. Parametric optimization

3.3.1. Statistical analysis through RSM model

In this investigation, the three most important operational parameters on selenium uptake, such as adsorbent dosage, Initial concentration, and contact duration, were taken as input variables, and the selenium removal (%) was considered as the outcome of this experiment design. The statistical coefficients for the model were generated using Expert Design Software 6.0, as shown in equation (17).

$$\begin{aligned}\%\text{Removal} = [&+37.58807 + 9.5901 * A - 0.671591 * B + 0.084659 * C \\ &+ 0.125000 * AB + 7.29972E - 17 * AC - 0.000250 * BC \\ &- 0.579545 * A^2 - 0.011932 * B^2 - 0.000169 * C^2]\end{aligned} \quad (17)$$

Where A is adsorbent dosage (g/L), B is contact duration (min), and C is selenium concentration (μg/L).

The analysis of variance (ANOVA) method was used to determine the impact of crucial parameters through model's regression equation. The equilibrium and initial selenium concentrations were computed to generate the actual data, and mathematical model equations were used to calculate the predicted values. Based on the actual and predicted data, the correlation coefficient (R^2) was calculated to validate the model's success.

Figure 6(a) shows the impact of contact time and adsorbent dose on selenium removal efficiency. The study showed that increasing the activated clay dose from 8 to 10 g l^{-1} and the contact period from 20 to 30 min improved the selenium removal rate from 80% to 92% while keeping an initial selenium concentration of 250 μg l^{-1}. Figure 6(b) indicates the relationship between selenium concentration, adsorbent dose, and removal efficiency. The study found that reducing the selenium initial concentration from 300 to 200 μg l^{-1} and increasing the adsorbent dose from 8 to 11 g l^{-1} improved the selenium removal rate from 86% to 92%. The contact time was kept constant at 30 min. Figure 6(c) presents the effect of selenium concentration and contact time on selenium removal efficiency. The study showed that decreasing the selenium concentration from 300 to 250 μg l^{-1} and the contact time from 40 to 30 min increased the removal efficiency from 88% to 90%. The adsorbent dose remained constant at 10 g l^{-1}. Throughout the experiments, other parameters such as pH (7), stirring speed (200 rpm), and temperature (25 °C) were kept constant. Another study by Badr *et al* in (2020) employed an adsorbent of green-synthesized AgNPs to remove selenium, obtaining a 265 mg g^{-1} capacity of selenium uptake with 10 mg l^{-1} of initial concentration, contact period of 1 h, and solution pH of 2. The ANOVA with various process parameters used activated clay as the adsorbent to validate the model. The ANOVA findings revealed an average removal effectiveness of 86.70, a standard deviation of 0.5878, and a coefficient of variation (COV%) of 0.6779. The model's correlation coefficient value (R^2) was determined to be 0.9931, while the adjusted and predicted R^2 values were 0.9869 and 0.9448, respectively. The close agreement

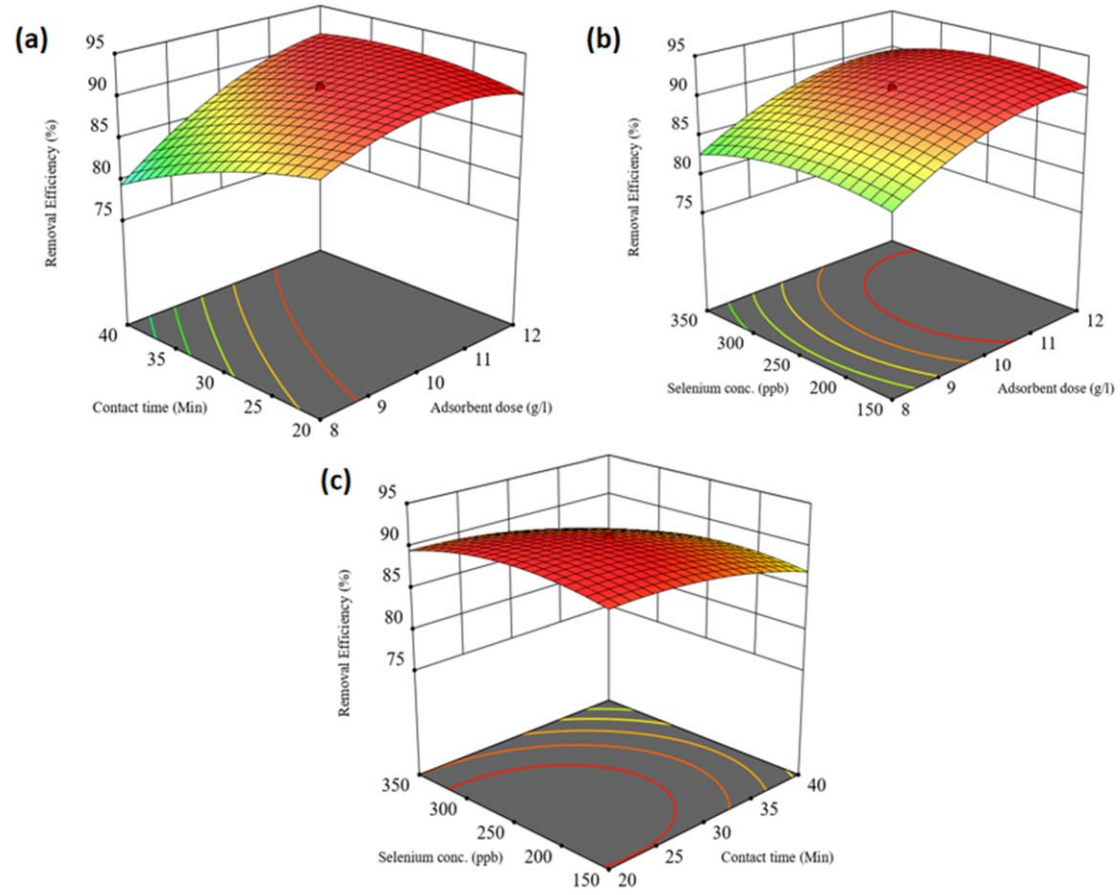

Figure 6. ANOVA-based analysis: (a) contact time and dose (b) Concentration and dose (c) Concentration and contact time.

between the adjusted R^2 of 0.9869 and the predicted R^2 of 0.9448, with a difference of less than 0.2, suggests the model's reliability. The ratio of 39.154 for adequate precision indicated that the model is effective in the design space, as it exceeds the desirable ratio of 4. Table 4 shows the actual and expected removal efficiency values estimated using the RSM model. Based on RSM analysis, it was found that 91% of selenium removal could be achieved within 30 min of contact time and an initial selenium concentration of 250 $\mu g\,l^{-1}$ while maintaining a pH of 7, a temperature of 27 °C, and a shaker speed of 200 rpm.

3.3.2. Statistical analysis through ANN model

In the present investigation, an ANN topology was developed, consisting of three nodes (neurons) in the input layer, corresponding to three input parameters, ten nodes in the hidden layer, and a single neuron in the output layer, representing the target data. The optimal number of nodes in the hidden layer was determined through a comprehensive optimization process involving multiple training configurations. This optimization aimed to minimize the MSE value and enhance the network's predictive performance and generalization ability for test factor values (Kumar *et al* 2024). The evaluation of the ANN model's performance in comparison to experimental results was conducted using statistical metrics. These metrics included the standard deviation (SD), mean, standard error, and COV. The SD quantifies the degree to which the ANN's output closely aligns with the experimental data stored in the database. Furthermore, the proximity of the mean value to unity, coupled with a modest standard deviation, serves as an indicator of the ANN network's capacity to generalize the data effectively. Conversely, the COV was employed to assess the precision of the ANN model outputs by highlighting the degree of data variability relative to the mean value. A lower COV signifies reduced data dispersion and greater model accuracy (Pranjal *et al* 2024).

It was proven beyond a reasonable doubt that ANN was adequate, as R^2 values close to 1 indicate a perfect correlation between experimentally obtained data and theoretically anticipated data (figure 7) (Streb & Mazzotti 2022). Ratio of (observed/predicted) was used to evaluate ANN prediction against pre-existing equations derived from an experimental database (Atta 2024). The standard deviation, the mean, and COV are obtained using the experimental/predicted ratio and are as follows:0.009587, 0.997708, and 0.9609%.

Table 4. Experimental design for various operational parameters using RSM and ANN model.

Std	Run	A: Adsorbent Dose (g/L)	B: Contact time (min)	C: Selenium Concentration (mg/L)	Actual removal efficiency (%)	Predicted removal efficiency: RSM (%)	Predicted removal efficiency: ANN (%)
3	1	8	40	150	81	78	78.23
15	2	10	30	250	90	91	90.99
9	3	6	30	250	73	75	75.00
16	4	10	30	250	90	91	90.99
4	5	12	40	150	91	90	90.00
17	6	10	30	250	90	91	90.99
6	7	12	20	350	89	88	88.00
19	8	10	30	250	92	91	90.99
11	9	10	10	250	91	90	90.00
1	10	8	20	150	88	87	90.90
5	11	8	20	350	85	86	86.00
18	12	10	30	250	90	91	90.99
10	13	14	30	250	85	89	89.00
13	14	10	30	50	86	86	86.00
8	15	12	40	350	88	88	88.00
12	16	10	50	250	83	83	83.00
7	17	8	40	350	78	76	76.00
2	18	12	20	150	89	89	89.00
20	19	10	30	250	89	91	90.99
14	20	10	30	450	83	83	83.00

3.4. Error analysis and model performance

Table 4 presents the anticipated responses generated by both ANN and RSM models alongside the observed responses obtained from experimental trials. The model effectiveness error evaluation illustrates the proposed model is relatively effective in anticipating the integrated system efficiency in terms of relative errors (RE), regression coefficients (R^2), and Willmott-d-index (d_{index}). All the error statistics in table 5 show low relative error (RE<0.10). However, the regression coefficient (R^2>0.97) and Willmott-d index (d>0.95) are relatively high, indicating that the model performs extremely well overall.

3.5. Adsorption isotherms and kinetics

Figure 8(a) illustrates the q_e and C_e relationship. The graph demonstrates that an increase in the initial concentration leads to a corresponding enhancement in the adsorbent's adsorption capacity. This phenomenon was observed at a temperature of 27 °C and a pH level of 7, where the equilibrium concentration was determined to be 250 $\mu g\,l^{-1}$. The Langmuir and Freundlich isotherm models, denoted in figures 8(a) and (b), respectively. Detailed parameters obtained from both isotherm models are presented in table 6. Notably, the Langmuir isotherm model exhibits a higher degree of fit with the adsorption isotherm data, as evidenced by its regression coefficient of 0.994, compared to the Freundlich isotherm model's coefficient of 0.984. The separation factor R_L was determined using equation (11), yielding values ranging from 0 to 1. This range indicates that the adsorption process is favorable and consistent with the Langmuir isotherm model. Figure 8(d) depicts the relationship between adsorption capacity qt and time t at any time. According to figure 8(d), the removal rate was extremely rapid in the initial adsorption phase. A contact period of 30 min is sufficient for optimal selenium removal, and increasing the contact time has no meaningful influence on efficiency. Figures 8(c) and (d) show the adsorption process's pseudo-order and second-order kinetic models. The first order and second parameters are listed in table 7. The graphical representation shows that the second-order kinetic model best fits the data, as the regression coefficient ($R^2 = 0.998$) is significantly higher than the first-order ($R^2 = 0.731$). According to the kinetic results in table 7, the observed value of adsorption capacity is near the calculated value in the second order but not in the first order.

The viability of adsorbate movement from the liquid state to the surface of the adsorbent via intra-particle diffusion was assessed using the intra-particle diffusion model. Figure 8(e) shows the plot between q_e and $t^{0.5}$. Table 6 shows the parameters obtained from plotting q_e against $t^{0.5}$. It was discovered that the regression coefficient R^2 was insufficient, indicating that the model did not follow the kinetics process. Therefore, we may conclude that the pseudo-second-order approach suggests a perfect match for the modeling of kinetic data.

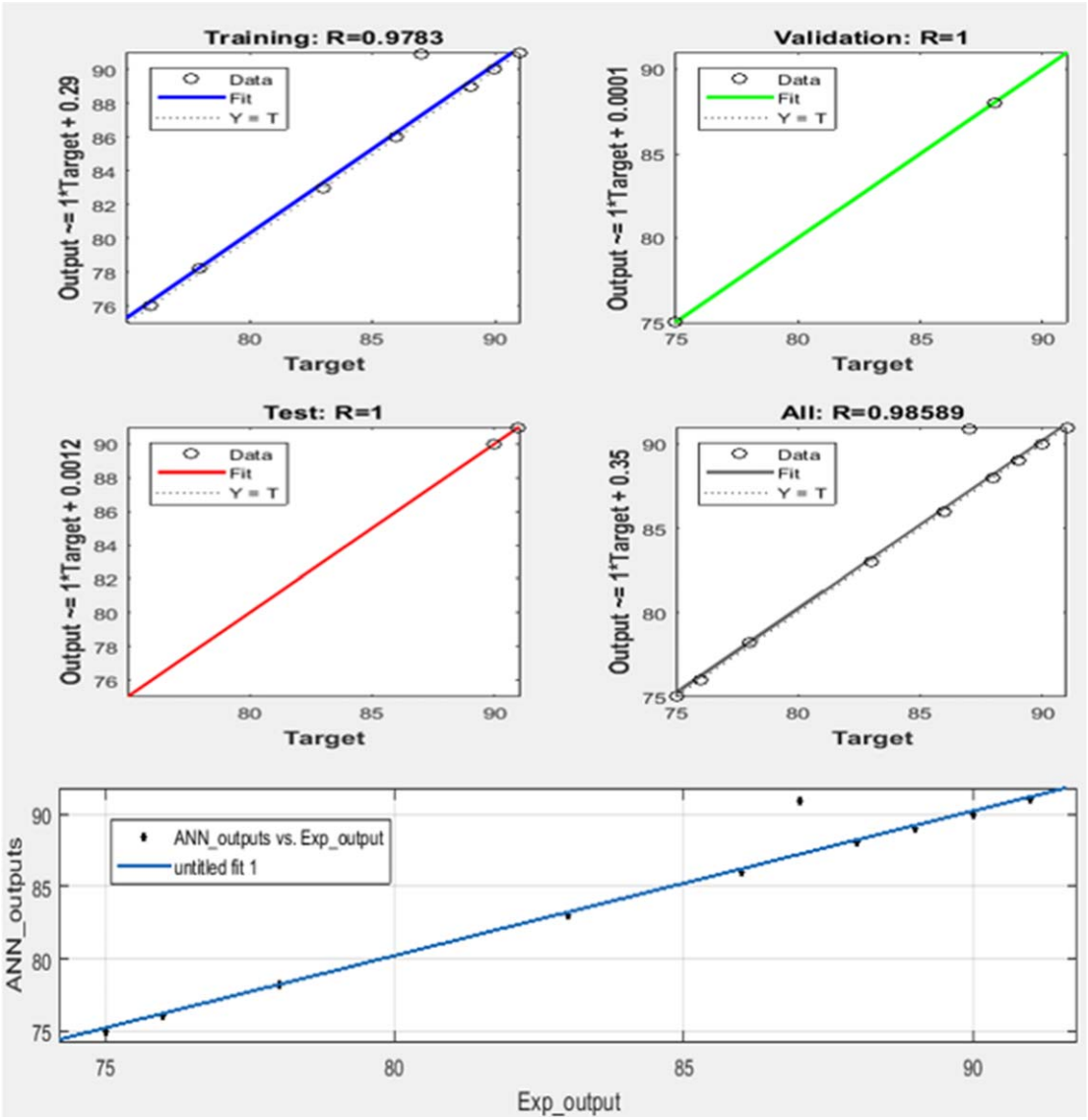

Figure 7. The Regression curve obtained after ANN training, testing, and validation.

Table 5. Model fitness assessments based on error analyses of selenium rejection.

Investigated models	Error parameters		
	RE	R^2	d_{will}
RSM	0.092	0.975	0.960
ANN	0.097	0.990	0.980

3.6. Adsorption thermodynamics

Thermodynamic parameters, including the Gibbs free energy change (ΔG°), enthalpy change (ΔH°), and entropy change (ΔS°), have been analyzed to assess the spontaneity of the adsorption process. The obtained results are presented in table 8. The determination of the Gibbs free energy change (ΔG°) via equation (15) has revealed a negative value, affirming the spontaneous nature of the adsorption process. As the temperature of the system increased from 298 to 328 K, it was observed that the free energy ΔG value decreased. This observation suggests that the inherent adsorption process occurs for both Se(IV) and Se(VI) (Monte *et al* 2017). Van't Hoff equation (16) and the graph between 1/T and $\ln K_L$ are used to evaluate the change in enthalpy (ΔH°) and entropy (ΔS°). An exothermic adsorption process was indicated by the negative normal enthalpy ΔH (-3.238 kJ mol^{-1}) for Se(VI), which showed that the process was spontaneous (Xue *et al* 2021).Heat energy is released during adsorption due to the force of attraction between the adsorbent and the adsorbate, making it an

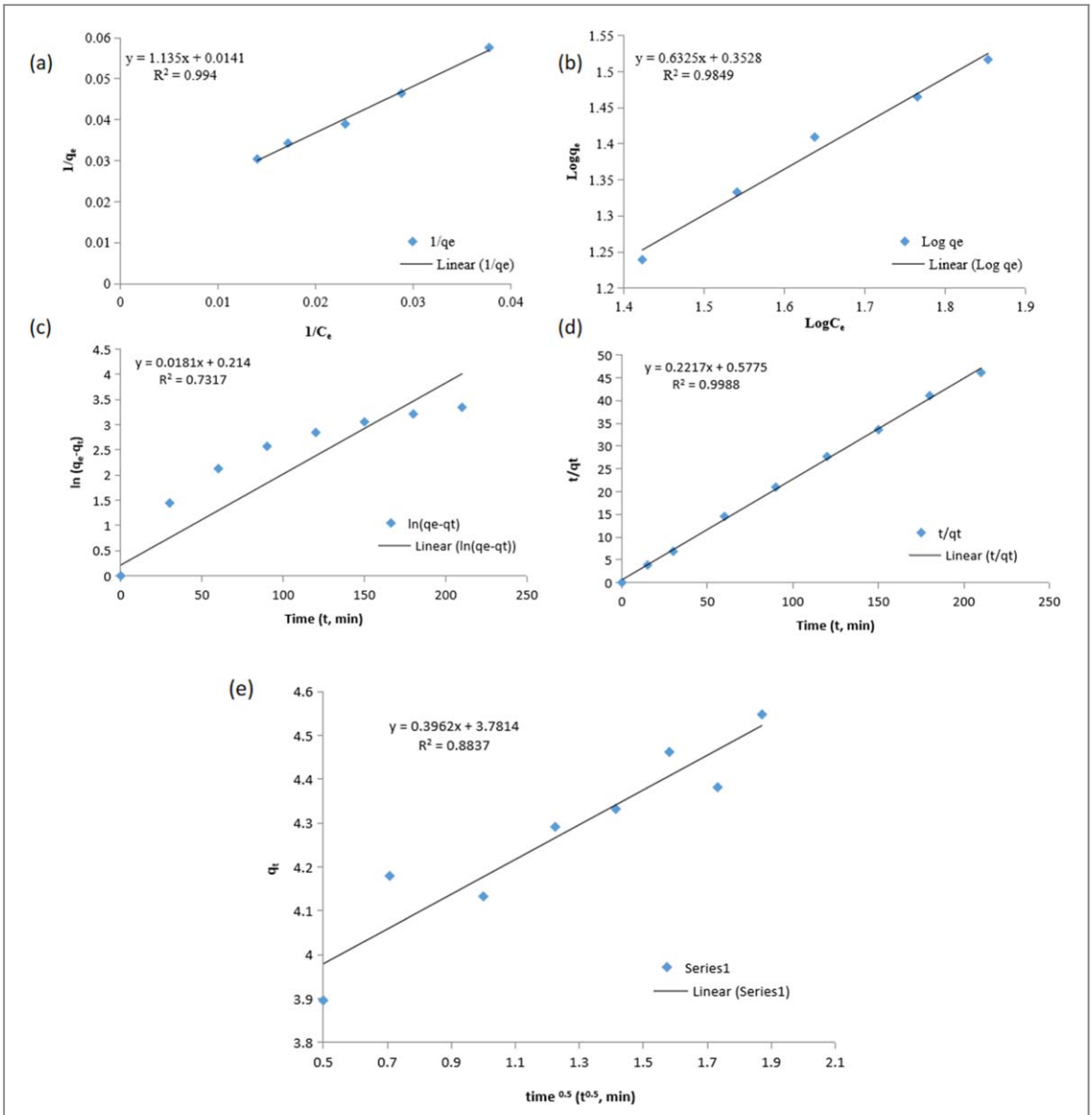

Figure 8. (a) Langmuir isotherm fitting (b) Freundlich isotherm fitting (c) Pseudo first order fitting (d) Pseudo second order fitting (e) effect of intra-particle diffusion.

Table 6. Adsorption isotherm parameters.

Langmuir isotherm parameters				Freundlich isotherm parameters		
q_m(μg/g)	K_L (L μ/g)	R_L	R^2	1/n	K_f (μg/g)	R^2
70.921	0.012	0.243	0.994	0.6325	2.250	0.985

Table 7. Adsorption kinetic parameters.

Pseudo-first-order kinetics				Pseudo-second-order kinetics				Intra-particle diffusion model		
K_1 (min^{-1})	q_e (calculated) (μg/g)	q_e (expected) (μg/g)	R^2	K_2 (min^{-1})	q_e (cal) (μg/g)	q_e (exp) (μg/g)	R^2	K_i (μg/g $h^{0.5}$)	C (μg/g)	R^2
0.0006	1.238	4.379	0.7317	0.085	4.51	4.379	0.999	0.331	3.88	0.626

exothermic reaction. The change of enthalpy obtained in this study is negative. Furthermore,A decline in the randomness of the particles is implied by the fact that the entropy change of the system is negative. An investigation conducted by Yang *et al* (2021) demonstrated that the Fe-OOH type adsorbent was effective in

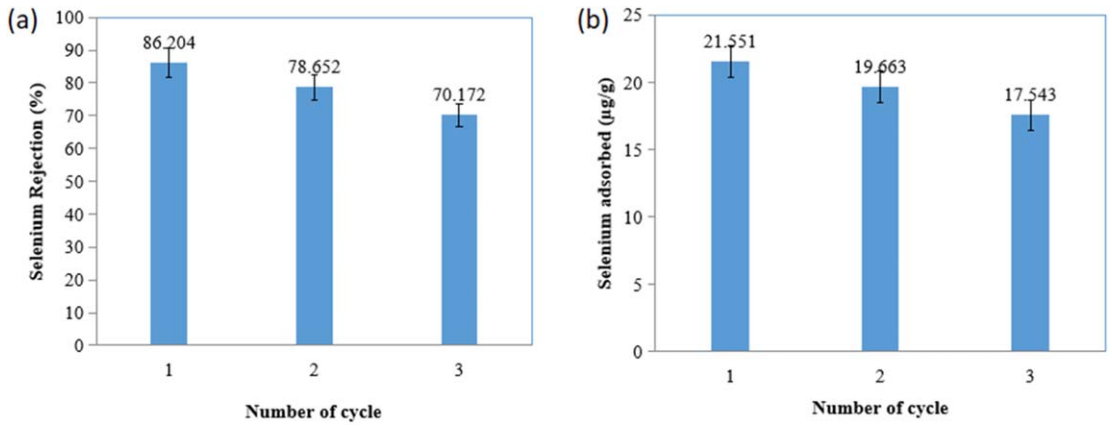

Figure 9. Selenium Regeneration performance analysis using preheated natural clay (i) selenium adsorbed (µg/g) in successive runs (ii) selenium rejection (%) in successive runs.

Table 8. Thermodynamic parameters of selenium uptake onto heated clay.

Temperature (K)	ΔG° (KJ/mol)	ΔH° KJ/mol K)	ΔS° (KJ/mol K)	R^2
298	−0.0806	−3.238	−10.598	0.9999
303	−0.02575	—	—	—
318	0.131864	—	—	—

removing Se(IV) and Se(VI) from water that had been contaminated. With regard to thermodynamic analysis, they have achieved results that are comparable to those found in their study (Yang *et al* 2021).

3.7. Regeneration study

In this study, we systematically investigated the regeneration and reusability potential of the newly developed adsorbent under optimal conditions. 250 $\mu g\,l^{-1}$ selenium solution was introduced into a 100 ml flask to assess its efficacy. The mixture was agitated in an orbital temperature-controlled shaker operating at 200 rpm for 30 min, maintaining a temperature of 27 °C and a pH of 7. An adsorbent dosage of 10 $g\,l^{-1}$ was employed in this experimental setup. Following each adsorption cycle, the solution underwent a 10-minute centrifugation at 2000 rpm. Subsequently, the separated material was carefully extracted from the centrifuge tube and dried in an oven set at 80 °C for one hour. The regeneration analysis encompassed four consecutive cycles, where we observed notable trends in the adsorption performance. Across these cycles, the adsorption loading capacity gradually declined, decreasing from an initial value of 21.5 micrograms per gram (µg/g) in the first cycle to 15.7 $\mu g\,g^{-1}$ in the fourth cycle. Similarly, the selenium rejection percentage declined from an initial value of 86.2% in the first cycle to 62.9% in the fourth cycle. These trends are visually represented in figure 9. Based on the outcomes of this investigation, it may be concluded that the regenerated produced adsorbent is unsuitable for further usage. It was noted that the second cycle of regeneration operation resulted in a reduction in selenium rejection from 86.2% to 78.65% with a residual concentration of 53.37 $\mu g\,l^{-1}$, which exceeds the allowable limit of 40 $\mu g\,l^{-1}$ for selenium levels in drinking water. As a result, the developed adsorbent is not recommended to be reused after the first cycle.

4. Economic analysis for the scale-up of the adsorption process

This part of the study has been investigated to scale up the adsorption process of selenium removal by activated natural clay. The overall cost of the efficient water treatment plant is divided into capital cost and operational cost. The capital cost of about 0.12 $\$/m^3$ was taken from the previous investigation, including civil cost, mechanical cost, and electrochemical for reducing inorganic pollutants using novel adsorbent material. The operational cost includes the preparation of adsorbent and electricity costs. The surface, morphology, and porous structure of the adsorbent material play a significant role in the adsorption process of activated natural clay, increasing removal efficiency. Therefore, one of the crucial factors to consider to keep the process of water treatment affordable for widespread application is the price of producing adsorbent material via several phases like collection of samples, washing, drying, reducing the size, the process of carbonization, activation process,

neutralization, and so on. A variety of factors influence the total cost of adsorbent materials, including accessibility, processing necessities, as well as treatment conditions, and recycling (Gupta and Suhas 2009). The total cost of adsorbent preparation has been investigated step by step to provide probable costs associated with the current research study. The process follows: Final cost of Adsorbent = Adsorbent Substance + Initial Drying + Activation (Thermal Treatment). Different cost components have been used in this study as follows:

1. Adsorbent material (1Kg) = 0.36$
2. Initial Drying = 0$
3. Activation cost = heating cost for activation = Holding time (hour) x units of power consumed x unit cost = $1.5 \times 4.5 \times 0.072 = 0.486$$
4. Total cost of producing adsorbent = 0.36+0+0.486 = 0.846$

The above step-by-step calculation gives an approximate idea that the total cost for producing 1 kg of natural clay material is 0.846, which is a lower price compared to commercial activated carbon 2.41$ for wastewater treatment. Therefore, this present techno assessment revealed a capital cost of 0.12$ and an operational cost of 0.846$, which is the total cost 0.9766$/$m^3$. The cost assessment results of this investigation using the novel material might be helpful for the long-term development of industrialization.

5. Conclusion

In conclusion, this study demonstrates the impressive potential of naturally heated clay as an efficient adsorbent for removing selenium from aqueous solutions. With 22.54 $\mu g\, g^{-1}$ of an optimum adsorption capacity, heated clay outperformed commercial adsorbents such as GAC and PAC, doubling their adsorption capacity. The batch experiments allowed us to identify the optimal operational parameters, including an adsorbent dose of 10 $g\, l^{-1}$, contact time of 30 min, starting concentration of 250 $\mu g\, l^{-1}$, shaker speed of 200 rpm, and pH 7. The kinetics adsorption and isotherms analysis revealed an excellent fit to the Pseudo second order & Langmuir isotherm models, indicating that the adsorption process is effective. The thermodynamic study further supported this, with negative values of ΔH° and ΔG° indicating that the adsorption process was exothermic and spontaneous, respectively. The negative ΔS° value implied a decrease in the system's unpredictability, enhancing confidence in the results. The RSM and ANN models showed promising results in predicting selenium removal efficiency, with ANN displaying slightly higher accuracy than RSM. However, the marginal errors between the models were minimal. The RSM model identified the best conditions for maximum efficiency, with 250 $\mu g\, l^{-1}$ of initial selenium concentration, an adsorbent dose of 10 $g\, l^{-1}$, and 30 min of contact time, achieving a close-to-91% removal efficiency, which was consistent with experimental results.

Furthermore, the models exhibited excellent performance even with previously unreleased data, confirming their generalization ability. The ANN model, in particular, demonstrated superior predictability compared to RSM. Overall, this study highlights the possibility of waste clay concerning low-cost and effective raw substances for developing an adsorbent capable of efficiently removing selenium from aqueous solutions. The findings offer valuable insights for addressing water contamination issues and provide a foundation for future water treatment and environmental sustainability research.

Acknowledgments

This work was supported by the National Research Foundation of Korea (NRF) grant funded by the Korean government (MSIT) (No. RS-2023-00219983). Moonis Ali Khan acknowledges the financial support through Researchers Supporting Project number (RSP2024R345), King Saud University, Riyadh. Saudi Arabia.

Data availability statement

All data that support the findings of this study are included within the article (and any supplementary files).

Conflicts of interest

There are no conflicts to declare.

ORCID iDs

Gude Ramesh https://orcid.org/0000-0002-2388-1109
Ramesh Kumar https://orcid.org/0000-0002-7150-4404
Byong-Hun Jeon https://orcid.org/0000-0002-5478-765X
Jayato Nayak https://orcid.org/0000-0001-7678-2019
Sankha Chakrabortty https://orcid.org/0000-0001-7719-8586

References

Al-Zahrani A A and Abdul-Majid M H 2009 Extraction of alumina from local clays by hydrochloric acid process *Engineering Science: Journal of King Abdulaziz University* **20** 29–41
Arslan M, Yılmaz M N, Günay K *et al* 2023 Removing selenite ions ($SeO3^{2-}$) from aqueous solutions by 4-vinyl pyridine monomer grafted poly(ethylene terephthalate) fibers and an estimation of its adsorption mechanism over pH dependency of the adsorption *Polym. Bull.* **80** 3135–52
Atta H A 2024 Artificial neural network [ANN] modeling for tetracycline adsorption on rice husk using continuous system *Desalin. Water Treat.* **317** 100026
Badawy N A, El-Bayaa A A and Abd AlKhalik E 2010 Vermiculite as an exchanger for copper(II) and Cr(III) ions, kinetic studies *Ionics* **16** 733–9
Badr N B E, Al-Qahtani K M and Mahmoud A E D 2020 Factorial experimental design for optimizing selenium sorption on Cyperus laevigatus biomass and green-synthesized nano-silver *Alexandria Engineering Journal* **59** 5219–29
Bibi I, Icenhower J, Niazi N K, Naz T, Shahid M and Bashir S 2016 Chapter 21-Clay Minerals: Structure, Chemistry, and Significance in Contaminated Environments and Geological CO2 Sequestration *Environmental Materials and Waste: Resource Recovery and Pollution Prevention* ed M N V Prasad and k Shih (Elsevier Inc.) pp 543–67
Bishayee B, Ruj B, Chakrabortty S and Nayak J 2021 Facile synthesis, characterization and application of heterogeneous Al@Si materials for adsorptive mitigation of fluoride: optimization and cost analysis *Environ. Nano. Mon. Manage.* **16** 100490
Biswas G, Thakurta S G, Chakrabarty J, Adhikari K and Dutta S 2018 Evaluation of fluoride bioremediation and production of biomolecules by living cyanobacteria under fluoride stress condition *Ecotoxicol. Environ. Saf.* **148** 26–36
Bleiman N and Mishael Y G 2010 Selenium removal from drinking water by adsorption to chitosan-clay composites and oxides: batch and columns tests *J. Hazard. Mater.* **183** 590e595
Chakraborty A K 2014 *Phase Transformations of Kaolinite Clay.* (Springer) 3-12, 43–7 185-206, 327-329
Chakraborty P and Halder G 2020 Ibuprofen sorptive efficacy of zirconium caged date seed derived steam activated alginate beads in a static bed column *RSC Adv.* **10** 24293–307
Crowley S 2007 Introduction to clay minerals - chemistry, origins, uses and environmental significance by B. Velde(Chapman and Hall) 1992. No. of pages: 198*Geol. J.* 29, 385–6
den Hartog S A M, Saffer D M and Spiers C J 2014 The roles of quartz and water in controlling unstable slip in phyllosilicate-rich megathrust fault gouges *Earth Planets Space* **66** 78–86
Djebbar M, Djafri F, Bouchekara M and Djafri A 2012 Adsorption of phenol on natural clay *Applied Water Science* **2** 77–86
Dobrowolski R and Otto M 2013 Preparation and evaluation of Fe-loaded activated carbon for enrichment of selenium for analytical and environmental purposes *Chemosphere* **90** 683e690
Freundlich H 1907 Über die Adsorption in Lösungen *Z. Phys. Chem.* **57U**
Gadsden A 1975 *Infrared Spectra of Minerals and Related Inorganic Compounds.* (The Butterworth group)
Gupta V K and Suhas 2009 Application of low-cost adsorbents for dye removal—a review *J. Environ. Manage.* **90** 2313–42
Hajjaji M, Kacim S, Alami A, El Bouadili A and El Mountassir M 2001 Chemical and mineralogical characterization of a clay taken from the Moroccan Meseta and a study of the interaction between its fine fraction and methylene blue *Appl. Clay Sci.* **20** 1–12
Hamid M, Abdulrahim Y, Liu D, Awad F N, Omer N A, Khan A and Huang K 2021 Selenium enriched yeast and Gum Arabic combination attenuate oxidative liver damage via suppression of oxidative stress, inhibition of caspase-3 and proinflammatory genes expression in carbon tetrachloride-intoxicated rats *Bioactive Carbohydrates and Dietary Fibre* **26** 100267
He Y, Xiang Y, Zhou Y, Yang Y, Zhang J, Huang H, Shang C, Luo L, Gao J and Tang L 2018 Selenium contamination, consequences and remediation techniques in water and soils: a review *Environ. Res.* **164** 288–301
Ho Y and McKay G 1999 Pseudo-second order model for sorption processes *Process Biochem.* **34** 451–65
Janz D M 2011 *Selenium.* (Academic) 31007–2
Kalaitzidou K, Bakouros L and Mitrakas M 2020 Techno-economic evaluation of iron and aluminum coagulants on Se(IV) removal *Water* **12** 672
Khan S, Ajmal S, Hussain T and Rahman M U 2023 Clay-based materials for enhanced water treatment: adsorption mechanisms, challenges, and future directions *Journal of Umm Al-Qura University for Applied Sciences.*
Kuan W H, Lo S L, Wang M K and Lin cf 1998 Removal of Se(IV) and Se(VI) from water by aluminum-oxide-coated sand *Water Res.* **32** 915e923
Kumar R *et al* 2024 Optimizing methanol synthesis from CO_2 using graphene-based heterogeneous photocatalyst under RSM and ANN-driven parametric optimization for achieving better suitability *RSC Adv.* **14** 12496–512
Kushwaha A, Goswami L, Lee J, Sonne C, Brown R J C and Kim K 2021 Selenium in soil-microbe-plant systems: sources, distribution, toxicity, tolerance, and detoxification *Crit. Rev. Environ. Sci. Technol.* 1–38
Lagergren S 1898 Zur theorie der sogenannten adsorption gelo ster stoffe *Kungliga Svenska Vetenskapsakademiens Handlingar, Band* **24** 1–39
Lamberov A A, Sitnikova E Y and Abdulga A S 2012 Kinetic features of phase transformation of kaolinite into metakaolinite for kaolin clays from different deposits *Russ. J. Appl. Chem.* **85** 892–7
Langmuir I 1918 The adsorption of gasses plane surfaces of glass, mica, and platinum *J. Am. Chem. Soc.* **40** 1361–403
Laub M, Blagodatsky S, Nkwain Y F and Cadisch G 2019 Soil sample drying temperature affects specific organic mid-DRIFTS peaks and quality indices *Geoderma* **355** 113897
Lu Z, Yu J, Zeng H and Liu Q 2017 Polyamine-modified magnetic graphene oxide nanocomposite for enhanced selenium removal *Separ. Purif. Technol.* **183** 249e257
Madejova J 2003 FTIR techniques in clay mineral studies *Vib. Spectrosc.* **31** 1–10

Mafu L D, Mamba B B and Msagati T A M 2016 Synthesis and characterization of ion imprinted polymeric adsorbents for the selective recognition and removal of arsenic and selenium in wastewater samples *J. Saudi Chem. Soc.* **20** 594e605
Malhotra M, Pal M, Chakrabortty S and Pal P 2023 A single functionalized graphene nanocomposite in cross flow module for removal of multiple toxic anionic contaminants from drinking water *Environ. Sci. Pollut. Res.* **30** 65250–66
Malhotra M, Pal M and Pal P 2020 A response surface optimized nanofiltration-based system for efficient removal of selenium from drinking Water *Journal of Water Process Engineering* **33** 101007
Mao M, Qi Y, Lu K, Chen Q, Xie X, Li X, Lin Z, Chai L and Liu W 2024 Selective capacitive recovery of rare-earth ions from wastewater over phosphorus-modified TiO_2 cathodes via an electro-adsorption process *Environmental Science & Technology* **58** 14013–21
Mark U, Anyakwo C N, Onyemaobi O O and Nwobodo C S 2019 Conditions for thermal activation of ngwo clay as an alternative resource for alumina *Natural Resources* **10** 1–15
Monei N L, Puthiya Veetil S K, Gao J and Hitch M 2021 Selective removal of selenium by phytoremediation from post/mining coal wastes: practicality and implications *Int. J. Min. Reclam. Environ.* **35** 69–77
Mora B P, Bertoni F A, Mangiameli M F, González J C and Bellú S E 2020 Batch and fixed-bed column studies of selenite removal from contaminated water by orange peel-based sorbent *Water Science and Engineering* **13** 307–16
Mourabet M, El Boujaady H, El Rhilassi A, Ramdane H, Bennani-Ziatni M, El Hamri R and Taitai A 2011 Defluoridation of water using Brushite: equilibrium, kinetic and thermodynamic studies *Desalination* **278** 1–9
Nigay P-M and Ange Nzihou T C 2017 The impact of heat treatment on the microstructure of a clay ceramic and its thermal and mechanical properties *Cera. Inter.* **43** 1747–54
Parida K M, Gorai B, Das N N and Rao S B 1997 Studies on ferric oxide hydroxides. III. Adsorption of selenite (SeO_3^{2-}) on different forms of iron oxyhydroxides *J. Colloid Interf. Sci.* **185** 355
Pommier A L, Simon S, Buzier R and Guibaud G 2019 Evaluation of a mercapto functionalized silica binding phase for the selective sampling of SeIV by diffusive gradients in thin films *Talanta* **199** 590–5
Pranjal *et al* 2024 Intensifying inactivation strategies: insights into the role of ultrasound on the inactivation of antibiotic resistant acinetobacter baumannii via Photo-Fenton reaction *Chem. Eng. J.* **497** 154670
Qureshi S S, Memon S A, Rafi-ul-Zaman *et al* 2022 Rapid adsorption of selenium removal using iron manganese-based micro adsorbent *Sci. Rep.* **12** 17207
Rovira M, Gimenez J, Martinez M, Martinez-Llado X, de Pablo J, Marti V and Duro L 2008 Sorption of selenium (IV) and selenium(VI) onto natural iron oxides: Goethite and hematite *J. Hazard. Mater.* **150** 279
Ruj B *et al* 2022 An economical strategy towards the managing of selenium pollution from contaminated water: A current state-of-the-art review *J. Environ. Manage.* **304** 114143
Streb A and Mazzotti M 2022 Performance limits of neural networks for optimizing an adsorption process for hydrogen purification and CO_2 capture *Comput. Chem. Eng.* **166** 107974
Su T, Guan X, Gu G and Wang J 2008 Adsorption characteristics of As(V), Se(IV), and V(V) onto activated alumina: effects of pH, surface loading, and ionic strength *J. Colloid Interface Sci.* **326** 347e353
Sun Q, Zhang W and Qian H 2016 Effects of high temperature thermal treatment on the physical properties of clay *Environ. Earth Sci.* **75** 610
Tang H, Li W, Jiang H, Lin R, Wang Z, Wu J and Brett D J L 2019 ZIF-8-derived hollow carbon for efficient adsorption of antibiotics *Nanomaterials* **9** 117
Torres J, Pintos V, Domínguez S, Kremer C and Kremer E 2010 Selenite and selenate speciation in natural waters: interaction with divalent metal ions *J. Solution Chem.* **39** 1–10
Wasewar K L, Prasad B and Gulipalli S 2009 Removal of selenium by adsorption onto granular activated carbon (GAC) and powdered activated carbon (PAC) *CLEAN - Soil, Air, Water* **37** 872–83
Weber T W and Chakravorti R K 1974 Pore and solid diffusion models for fixed-bed adsorbers *AlChE J.* **20** 228–38
World Health Organization 2011 *Guidelines for Drinking-water Quality* 4th ed.
Zendehdel M, Shoshtari-Yeganeh B, Khanmohamadi H and Cruciani G 2017 Removal of fluoride from aqueous solution by adsorption on NaP: HAp nanocomposite using response surface methodology *Process Saf. Environ. Prot.* **109** 172–91
Zhang S, Tan D, Zhu H, Pei H and Shi B 2024 Rheological behaviors of Na-montmorillonite considering particle interactions: a molecular dynamics study *Journal of Rock Mechanics and Geotechnical Engineering.* Accepted,
Zhao Y-G, Chen L-H, Ye M-L, Su W-S, Lei C, Jin X-J and Lu Y 2024 U(VI) removal on polymer adsorbents: Recent development and future challenges *Critical Reviews in Environmental Science and Technology* 1–23
Zheng S, Su J, Wang L, Yao R, Wang D, Deng Y, Wang R, Wang G and Rensing C 2014 Selenite reduction by the obligate aerobic bacterium Comamonas testosteroni S44 isolated from a metal-contaminated soil *BMC Microbiol.* **14** 1–14
Zoroufchi Benis K, Motalebi Damuchali A, McPhedran K N and Soltan J 2020b Treatment of aqueous arsenic - a review of biosorbent preparation methods *J. Environ. Manag.* **273** 111126
Zoroufchi Benisa K, McPhedran K N and Soltan J 2022 Selenium removal from water using adsorbents: a critical review *J. Hazard. Mater.* **424** 127603